The 2010 IEEE/RSJ International Conference on
Intelligent Robots and Systems
October 18-22, 2010, Taipei, Taiwan

Acquisition of Tactile Information by Vision-based Tactile Sensor for Dexterous Handling of Robot Hands

Yuji Ito, Youngwoo Kim, Chikara Nagai, and Goro Obinata

Abstract—**In this paper, we propose a new method for calculation of the contact region and the location of an object from the data acquired from vision-based tactile sensor, which touch pad is an elastic transparent membrane of silicon rubber with dotted pattern printed on its inner side. The membrane is filled with translucent red colored water. The algorithm for calculation of the contact region is based on the curvature radius of the elastic membrane and considerations of the conditions for balance between the tensional forces of the membrane and the inner pressure. The location of the object is calculated from the relations between the translational displacement of the object and the displacement of the contacting dots. The rotation angles of the object are estimated from the rotation matrix of the three basis vectors by accumulating changes of the rotation angles of the rotation matrix for applying to the object rolling on the sensor. This paper also provides some experimental results that demonstrate the usefulness of the proposed method. Proposed method can be applied in many robot tasks that require dexterity of the robot hands.**

I. Introduction

TACTILE receptors in the skin allow human to sense contact with objects, contact force, slippage of grasped object, shape and irregularity of the contact surface, temperature of the object, air flow, etc. Precise muscle control and dexterity of the human hand are due to the feedback information from tactile receptors. Tactile information is essential component of robot control system. Quality of the tactile sensors is a key factor that determines the efficiency of the robot in the completion of tasks that require dexterity of the robot hands and precise objects handling.

In many robots, tactile sensing system is organized as a complex array of single sensors mounted to the robotic gripper. Various tactile sensing concepts based on single sensors (resistive, capacitive, piezoelectric, ultrasonic, electromagnetic, etc) have been introduced so far. Serious drawback of such solutions is that they require wiring in the contact surface which reduces the reliability of the system and increases the price of the robot. Differently from that, vision-based sensors can be fabricated compact in size and structure [1] and do not require wiring. K. Kamiyama et al. proposed a tactile sensor based on elastic body with double-layered dotted patterns printed on it. CCD camera is used to capture the image of the dotted array and the displacement of the dots is used for calculation of the forces applied to the elastic body [2]. Optical sensors from that type acquire only specific type tactile information which limits their application.

Modern robot design demands sophisticated tactile sensors that can measure the contact forces in many points and sense the shape and surface irregularity of the grasped object. Tactile information about the object shape allows the robot control system to choose grasping strategy when robot fingers conform to the shape of the grasped object. Force information is essential for choosing the right grasping force when the object is grasped strong enough to prevent eventual slippage but the force applied to the same object does exceed the limits that cause such object to collapse or being damaged. S. Saga et al. developed an optical tactile sensor that uses transparent silicone rubber as a deformable mirror surface. The reflection image changes on different way depending on the magnitude of the force and the position of its application [3]. The sensor is proposed by N. J. Ferrier et al uses a grid of dots drawn on the inner surface of a latex membrane. The grid image changes when the membrane enters in contact with the object [4]. R. Miyamoto proposed sensing of the shape of objects by elastic body with embedded force sensors [5]. K. Nagata et al. developed a rubber skin that provides information about the shape of the object. The design includes a pin array, CCD camera and light source on its inner side [6]. The CCD camera captures the image of the pin array and associated changes caused by deformation of the rubber skin

Sensors from that group provide information about the shape of the object but they cannot give information about the contact region between the sensor and the object. In order to avoid the risk that the membrane tears or the grasped object collapses, we also need to evaluate the contact pressure.

Precise manipulation tasks that involve grasping and rolling of the object require information about the exact location which is the position and orientation of the object to the robotic hand. Various sensors for detection of the object location have been proposed. Y. Yamada et al. developed a robot skin that uses tiny reflector chips arranged in a matrix form on the elastic sensor surface to inform about the exact location of the object [7]. Proposed sensing method gives information about the position and orientation of the object. However, the sensor cannot give enough information about the orientation of objects with uniform shapes such as sphere

Manuscript received July 15, 2010.

Yuji Ito and Chikara Nagai are with Graduate School of Engineering, Nagoya University, Furo-cho, Chikusa-ku, Nagoya, 464-8603, Japan.

Youngwoo Kim and Goro Obinata are with EcoTopia Science Institute, Nagoya University, Furo-cho, Chikusa-ku, Nagoya, 464-8603, Japan; e-mail: obinata@mech.nagoya-u.ac.jp.

or cylinder.

Obinata et al proposed tactile sensor and a method for simultaneous acquisition of information about shape/irregularity of the object, contact force/moment, and slippage intensity [8][9][10]. In this paper, we propose a new method to calculate the contact region of the sensor, and the location of the object, where the previously developed sensing method can be applied in conjunction with the proposed method.

II. VISION-BASED TACTILE SENSOR

A. Vision-based Tactile Sensor

Fig.1 shows the configuration of the vision-based tactile sensor. It consists of CCD camera, LED lights, transparent acrylic plate, and touch pad shaped as an elastic membrane of silicon rubber. Translucent red colored water fills the membrane. For the experiments we used a CCD camera with dimensions 8 × 8 × 40 mm and LED lights dimensioned as 60 × 60 × 60 mm.

The touch pad has semispherical shape. Its curvature radius is 20 mm and the height is 13 mm. The touch pad has two-layered structure. The outer membrane is black, while the inner membrane is white, as shown in Fig.2. Elastic membranes of silicon rubber with thickness of 0.5 mm have been used for each layer. Dotted pattern is printed on the inner membrane. Dots have diameter of 0.7 mm and the distance between two neighbor dots of the array is 1.5 mm. The LED source uses a polarized light filter to eliminate the light reflected from the transparent acrylic plate and to produce uniform light beam directed in parallel to the image capturing direction.

The CCD camera takes images with sampling frequency of 30 Hz of the inner spherical surface of the touch pad through the acrylic plate. Fig.3 shows the shape of the captured images. Each image frame has 640 pixels × 482 effective pixels. Fig.3 (a) shows the captured image when the sensor is not in contact with the object. Fig.3 (b) shows the image when the sensor is in contact with an object.

B. Measurement of the Contact Force and Moment

We can measure the normal force, tangential force and moment in the area of contact based on the analysis of movement of dots and the contact region.

The brightness of a pixel in the image changes when the corresponding area is in contact with the object. This is used for calculation of the shape and size of the contact surface. The relation between the contact surface and applied normal force can be found experimentally. Then, the lookup table can be used to calculate the normal force acting to the sensor. Details about experimental verification of that approach can be found in [8]. The tangential force and the moments applied to the sensor in the contact area can be calculated by analysis of the displacements of the dots on the contact area. The algorithms for calculation are reported in [8].

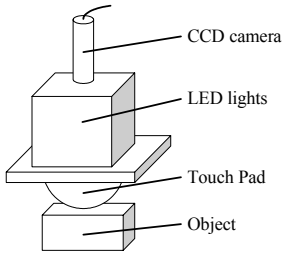

Fig. 1. Configuration of vision-based tactile sensor.

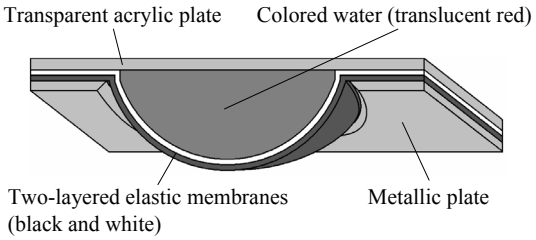

Fig. 2. Configuration of proposed touch pad.

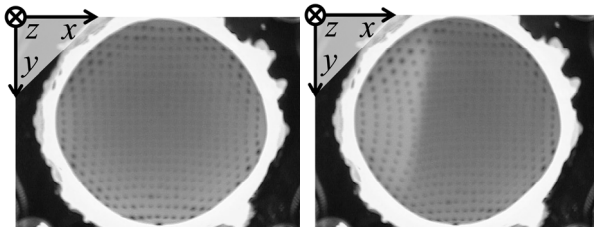

(a) (b)

Fig. 3. Captured images; (a) is non-contact state. (b) is contact state.

C. Estimation of Slippage Degree

Events of slippage of an object can be detected by analysis of sequential frames of the dotted patterns.

The image of the contact surface is divided into two regions. When the tangential force is smaller than the friction resistance the sensor surface sticks to the object. The image that corresponds to that state defines a region that is called stick region. When the tangential force becomes bigger than the friction resistance, the incipient slippage occurs. This state forms a region called slippage region. When humans grasp an object with their fingers, these two regions are sensed by several receptors in the cutaneous sensory system and provide feedback about the slippage degree and the motor system responds with increasing of the finger pressure to avoid the macroscopic slippage. Slippage degree can be found by analysis of the relative displacement of each dot of the image. The method was introduced in [9]. In this study, we assume that the displacement of the object is the same as the displacement of the reference dot. The reference dot is defined as the dot that is nearest to the center of the stick region. The ratio between the sizes of the stick region and total contact region is called the stick ratio (ϕ). States of slippage and collapsing of the grasped objects can be detected easily by the value of the stick ratio.

III. Estimation of Tactile Information

A. Shape Sensing

The intensities of the lights color components (red, green and blue) in the image captured with the CCD camera can provide information about the distance from the acrylic plate to the touch pad is estimated for each pixel and thus, about the shape of the object and irregularity of the object surface. The pixels look red since they are seen through the red water that fills the membrane. However, the darkness of each pixel is different depending on the distance to the inner membrane. When the distance is small the pixel looks light red. Pixels that represent bigger distances to the membrane surface are dark red colored. Algorithm for estimation of the distance to the membrane surface was introduced in [10]. The reflection and scattering coefficients were decoupled in the proposed formulation and the intensity of traveling light was represented as a function of the geometrical parameters of the pad surface. Developed mathematical model excluded certain factors because of simplicity concerns. The errors caused by the excluded parameters were minimized by development of a compensation procedure based on the shape of the membrane.

B. Estimation of the Contact Region

As introduced in the previous chapter, the dependable shape sensing of an object is confined to the contact region. Therefore, defining of the contact region of the object is essential. The deformation of the elastic membrane may occur either as a result of contact of the object or in situations when the tensional force of the (noncontact) membrane and the inner pressure of the touch pad are balanced. That's why it is difficult to conclude from shape of the touch pad whether the object is in contact with the touch pad.

In this study we estimate the contact region by analysis of the curvature radius of the elastic membrane. As a result of the tensional force and inner pressure, the elastic membrane should bulge outward from the contact region. The effect of the tensional force and inner pressure on a small segment of the membrane is illustrated in Fig.4. The inner pressure p is described based on Young–Laplace equation as follows.

$$\left(\frac{\sigma_1}{R_1}+\frac{\sigma_2}{R_2}\right)=p \tag{1}$$

where σ_1 and σ_2 are the tensional forces per unit length of the membrane, and R_1 and R_2 are the curvature radiuses of the elastic membrane. The equation (1) is applied to the concave segments of Fig.5 (a) as follows.

$$\left(\frac{\sigma_1}{R_1'}+\frac{\sigma_2}{R_2'}\right)=p \tag{2}$$

where R'_i (i=1, 2) is R_i when the segment is convex, while R'_i is $-R_i$ when the segment is concave. Since the pressure p must

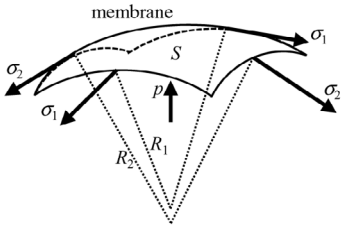

Fig. 4. Tensional force - inner pressure relation on a convex membrane.

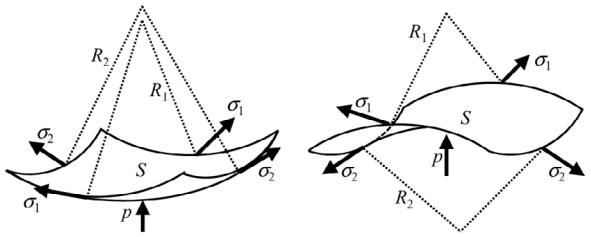

Fig. 5. Tensional force - inner pressure relation on concave membrane.

be positive, the flat or concave segment of the membrane does not satisfy (2) and the contact forces should be applied to set the membrane in balanced state. Therefore, we can consider the segment to belong to the contact region if the values of R'_i are 0 or negative. However, the curvature radiuses obtained from the shape of the membrane may contain estimation error. For that reason in this study we consider all segment which R'_i satisfies (3) as belonging to one in the contact region.

$$\frac{1}{R_i'}<\delta \ (i=1,2) \tag{3}$$

$$\delta > e_i \ (i=1,2) \tag{4}$$

Here, δ is a threshold value which is set to be always larger than the estimation error e_i. The estimation error e_i is defined as the difference between the estimated R'_i and the actual R'_i. However, equations (3) and (4) use only two curvature radiuses. Because of that, condition (3) has a directional dependence. The error from the directional dependence can be decreased if (3) and (4) are modified to (5) and (6) as follows.

$$\frac{1}{R_{i,j}'}<\delta \ (i=1,2,\ j=1,2,...,n) \tag{5}$$

$$\delta > e_{i,j} \tag{6}$$

In the above relation we use j indexes to note the curvature radius direction. R'_{ij} is the curvature radius.
We assume that ($\sigma > \sigma_1$, $\sigma > \sigma_2$), where σ is larger than σ_1 and σ_2. That modifies (2) into the following form:

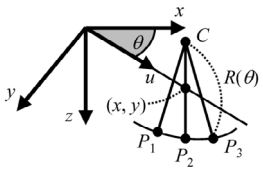

Fig.6. The curvature radius in the *u*-*z* plane.

$$\frac{1}{2}\left(\frac{1}{R'_{1,j}}+\frac{1}{R'_{2,j}}\right)>\frac{p}{2\sigma}\quad(\sigma>\sigma_1,\sigma>\sigma_2)\,(j=1,2,...,n)\qquad(7)$$

Note that it is possible for the segment to satisfy both (5) and (7) when $p/2\sigma$ is smaller than δ. If δ is small enough, the conditions (5) and (7) are not easily satisfied simultaneously. In order to decrease δ, the condition (5) which the convex segment must satisfy the following condition:

$$\frac{1}{n}\sum_{j=1}^{n}\left(\frac{1}{R'_{1,j}}+\frac{1}{R'_{2,j}}\right)<\delta\qquad(8)$$

where

$$\delta>\frac{1}{n}\sum_{j=1}^{n}\left(e_{1,j}+e_{2,j}\right).\qquad(9)$$

The value of δ when calculated with (9) is smaller than the δ calculated with condition (6) because $\Sigma(e_{1,j}+e_{2,j})/n$ in (9) is significantly smaller than $e_{i,j}$ in (6). Although this method can be applied successfully to the cases of Fig.4, and Fig.5 (a), it will give estimation error if applied to case of Fig.5 (b), when the membrane is complexly deformed. We can obtain the contact region in an accurate manner if we take smaller segment size.

Next, we obtain the curvature radiuses in $2n$ different directions by calculating the curvature radius of the each segment of the membrane. The curvature radius of the membrane is measured in the *u*-*z* plane which is perpendicular to the *x*-*y* plane as shown in Fig.6, where u is the direction on *x*-*y* plane. In order to obtain the curvature radius at $(x, y, l(x, y))$, we assume that the shape of a small segment around $(x, y, l(x, y))$ of the membrane is circular in an arbitrary *u*-*z* plane. The curvature radius can be defined by three points P_1, P_2, and P_3 that lie on them. The reference points have coordinates: $P_1(x\text{-}r\cos\theta,\ y\text{-}r\sin\theta,\ l(x\text{-}r\cos\theta,\ y\text{-}r\sin\theta,))$, $P_2(x,\ l(x,\ y))$ and $P_3(x+r\cos\theta,\ y+r\sin\theta,\ l(x+r\cos\theta,\ y+r\sin\theta,))$ which are obtained by using the shape estimation method [10]. From their coordinates we define the following equations that describe the membrane circular segment:

$$(x-c_{x\theta})^2+(y-c_{y\theta})^2+(z-c_{z\theta})^2=R(\theta)^2\qquad(10)$$

$$\frac{y-c_{y\theta}}{x-c_{x\theta}}=\tan\theta\qquad(11)$$

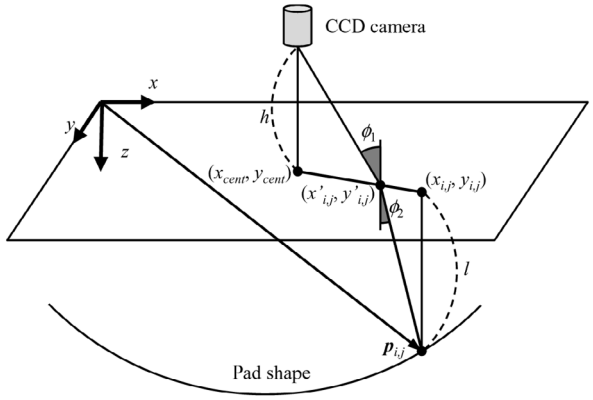

Fig.7. Geometrical relationship between the three- dimensional dot position and the one in the captured image.

where point $C(c_{x\theta}, c_{y\theta}, c_{z\theta})$ is the center of the circle and $R(\theta)$ is the curvature radius in the *u*-*z* plane in Fig.6.

Finally, the criteria for a segment to belong to the contact region is obtained by substituting $R(\theta)$ into (8) as follows.

$$\frac{1}{n}\sum_{j=1}^{n}\left\{1\Big/R'\left(\frac{\pi j}{2n}\right)+1\Big/R'\left(\frac{\pi j}{2n}+\frac{\pi}{2}\right)\right\}<\delta\qquad(12)$$

C. Estimation of Object Location

In order to estimate the location of the object, we focus on the positions of the dots printed on the inner membrane. The three-dimensional positions of dots are obtained by using the geometrical relationship as presented in Fig.7. That leads to the following equation:

$$\boldsymbol{p}_{i,j}=\begin{bmatrix}x_{i,j}\\ y_{i,j}\\ z_{i,j}\end{bmatrix}=\begin{bmatrix}\left(x'_{i,j}-x_{cent}\right)\left(1+l\sin\phi_2/h\tan\phi_1\right)+x_{cent}\\ \left(y'_{i,j}-y_{cent}\right)\left(1+l\sin\phi_2/h\tan\phi_1\right)+y_{cent}\\ l\left(x_{i,j},y_{i,j}\right)\end{bmatrix}\qquad(13)$$

where $\boldsymbol{p}_{i,j}$ is the position vector of the dot i, j , that is i-th dot from the left and j-th dot from the top. $x_{i,j}$, $y_{i,j}$ and $z_{i,j}$ are the position of $\boldsymbol{p}_{i,j}$ in the Cartesian coordinates, respectively. $x'_{i,j}$ and $y'_{i,j}$ are the dot positions in the captured image. $l(x_{i,j}, y_{i,j})$ is the depth of the pad at point $(x_{i,j}, y_{i,j})$ and h is the distance between the camera and the acrylic plate. x_{cent} and y_{cent} are the center positions of the captured image. We define contact reference dot $\boldsymbol{p}_{I,J}$. This is the dot which displacement from the initial position is biggest. The contact reference dot should be always in contact with object. When the object doesn't slip, the displacement of the object is equal to that of the contact reference dot, although the translational and rotational displacements of the object are not identified.

Next, we obtain the relative orientation of the object in reference to the orientation when it starts to contact with the sensor. The rotation angle of the object is equal to the rotation angle of the segment around the contact reference dot when the object doesn't slip. In order to obtain the rotation angle of

the contact reference dot, we estimate the rotation matrix $\boldsymbol{R}$ around the contact reference dot. Here, we assume that the eight dots adjacent to the contact reference dot are in continuous contact with the object. When the object does not slip the relative positions and the relative orientations of these eight points to the contact reference dot stay the same. In order to calculate the rotation angles of the contact reference dot, we define three basis vectors $\boldsymbol{n}_1$, $\boldsymbol{n}_2$ and $\boldsymbol{n}_3$ around the contact reference dot on the following way:

$$\boldsymbol{n}_1 = \sum_{k=-1}^{1}\left(\boldsymbol{p}_{I+1,J+k} - \boldsymbol{p}_{I-1,J+k}\right) \Big/ \left|\sum_{k=-1}^{1}\left(\boldsymbol{p}_{I+1,J+k} - \boldsymbol{p}_{I-1,J+k}\right)\right| \tag{14}$$

$$\boldsymbol{n}_2 = \sum_{k=-1}^{1}\left(\boldsymbol{p}_{I+k,J+1} - \boldsymbol{p}_{I+k,J-1}\right) \Big/ \left|\sum_{k=-1}^{1}\left(\boldsymbol{p}_{I+k,J+1} - \boldsymbol{p}_{I+k,J-1}\right)\right| \tag{15}$$

$$\boldsymbol{n}_3 = \boldsymbol{n}_1 \times \boldsymbol{n}_2 \tag{16}$$

The relation between $\boldsymbol{n}_1$, $\boldsymbol{n}_2$ and $\boldsymbol{n}_3$ in the k-th image and l-th image is represented as follows.

$$\begin{bmatrix} \boldsymbol{n}_1^l \\ \boldsymbol{n}_2^l \\ \boldsymbol{n}_3^l \end{bmatrix} = {}^k\boldsymbol{R}^l \begin{bmatrix} \boldsymbol{n}_1^k \\ \boldsymbol{n}_2^k \\ \boldsymbol{n}_3^k \end{bmatrix} \tag{17}$$

In the above equation we use l and k to note the sampling indexes of the image. ${}^k\boldsymbol{R}^l$ is the matrix that represents the rotation between the k-th and l-th images. It is obtained by multiplying both sides of (17) by $[\boldsymbol{n}_2, \boldsymbol{n}_2, \boldsymbol{n}_3]^{-T}$. The rotation angles around x, y and z-direction ${}^k\theta^l_x$, ${}^k\theta^l_y$ and ${}^k\theta^l_z$ between the k-th and l-th images are calculated by solving the following equation

$${}^k\boldsymbol{R}^l = {}^k\boldsymbol{R}^l_z\,{}^k\boldsymbol{R}^l_y\,{}^k\boldsymbol{R}^l_x \tag{18}$$

where ${}^k\boldsymbol{R}^l_x$, ${}^k\boldsymbol{R}^l_y$ and ${}^k\boldsymbol{R}^l_z$ are the rotation matrixes around x, y and z-direction, respectively. Note that the orientation of the object is not equal to ${}^k\theta^l_x$, ${}^k\theta^l_y$ and ${}^k\theta^l_z$ because the contact reference dot may be changed in some situations such a rolling of the object. The orientation angles of the object ${}^m\theta^n_{objx}$, ${}^m\theta^n_{objy}$ and ${}^m\theta^n_{objz}$ can be calculated as the sums of the values of ${}^k\theta^{k+1}_x$, ${}^k\theta^{k+1}_y$ and ${}^k\theta^{k+1}_z$ from each image captured by the CCD camera:

$${}^m\theta^n_{obj\,x} = \sum_{k=m}^{n-1} {}^k\theta^{k+1}_x,\ {}^m\theta^n_{obj\,y} = \sum_{k=m}^{n-1} {}^k\theta^{k+1}_y,\ {}^m\theta^n_{obj\,z} = \sum_{k=m}^{n-1} {}^k\theta^{k+1}_z \tag{19}$$

IV. Experimental Results

In the section we provide two examples for estimation of the contact region of the touch pad and location of the object that use the method presented in the previous section.

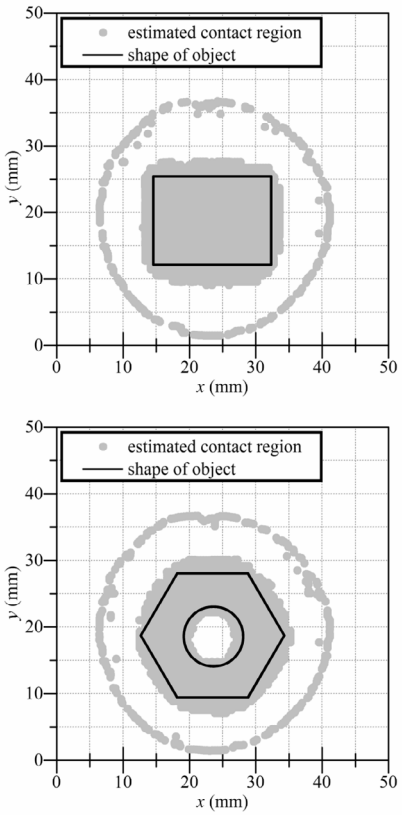

Fig.8. Estimation results of the contact region: (a) is square shape. (b) is hexagon bolt.

A. Estimation of Contact Region

Fig.8 (a)(b) shows experimental results of the estimation of the contact region between the touch pad and the object when the object is in contact with the sensor and the force applied to the sensor is parallel to z direction. Parameters δ, n and r are determined as 0.00015 (mm^{-1}), 18 and 10 pixel which were obtained experimentally.

B. Estimation of Object Location

We did an experiment when an object is in contact with the sensor and moves within the x-z plane. The position of the object was calculated by the method described in III.C. For comparison, we measured also the actual position of the objects. Fig.9 shows the experiment result. The upper graph shows the position of the object in the x direction. The lower graph shows the position of the object in z direction at the corresponding sampling time of the captured image. In order to obtain the actual object position, we installed a side camera which takes images of the side surface of the touch pad as shown in Fig.10. The results show that the object position is successfully estimated. The position of the contact reference dot was used in the calculations. Maximum errors do not exceed 0.3 mm in x-direction and 0.4 mm in z-direction. These errors occurred because of the variation of the shape estimation [10].

During the test for estimation of the object orientation the

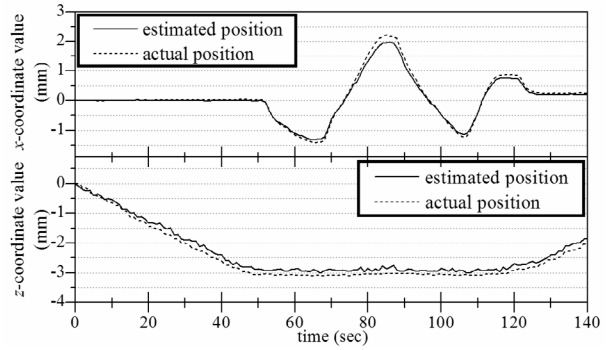

Fig.9. Estimation results of the object position.

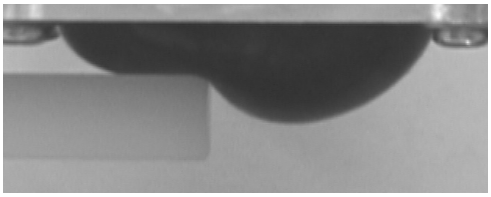
Fig.10. Side surface image of the touch pad.

object moves in z direction and rotates around the x axis. The actual angle around x axis of the touch pad was obtained from the image captured by camera directed to the side surface of the sensor. Experimental results are shown in Fig.11. The object orientation was estimated by using the rotation matrix of the three basis vectors as defined in section III.C. The maximum error is caused by the variation of the shape estimation and does not exceed 3 deg,

In Fig.12 we provide result from the estimation of the object orientation when the object rolls and contacts at the same time with the touch pad. In such experiment contact reference dot frequently changes. Despite of that, the sensor accurately estimates the rotation angle of the object by accumulating changes of the rotation angle of the contact reference dot. This shows that the orientation estimation method can be applied also in tasks when the contact region is changing.

V. Conclusion

In this paper, we have proposed a new method to estimate the contact region of the sensor, and the location of the object by using vision-based tactile sensor. We focused on the curvature radius of the elastic membrane to estimate the contact region, considering the balance between the tensional forces of the membrane and the inner pressure. In order to decrease the directional dependence of objects and the threshold value δ of the maximum estimation error we used the curvature radiuses in many different directions. The location of the object was obtained by using the dot positions. The translational displacement of the object corresponded to the displacement of the contact reference dot. The rotation angles of the object were calculated from the rotation matrix of the three basis vectors by accumulating changes of the rotation angles of the rotation matrix. We provide some experimental results that confirm the practicality of the

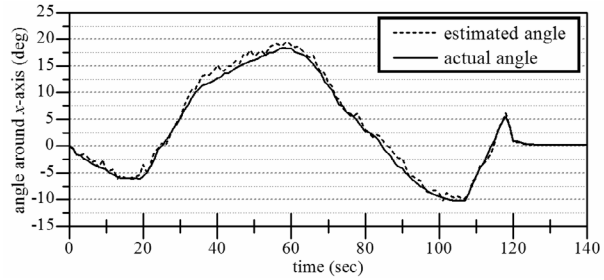

Fig.11. Estimation results of the object orientation.

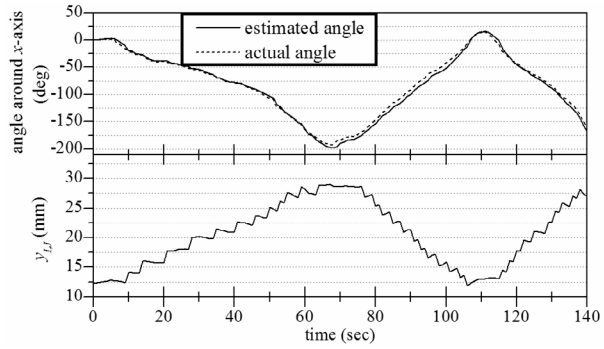

Fig.12. Estimation results of the object orientation when object rolls.

method. Future work includes the implementation of the developed sensor to a robot hand.

References

[1] M. H. Lee and H. R. Nicholls, "Tactile sensing for mechatronics-a state of the art survey" *Mechatronics*, 9, pp. 1–31, Jan, 1999

[2] K. Kamiyama, K. Vlack, T. Mizota, H. Kajimoto, N. Kawakami and S. Tachi, "Vision-Based Sensor for Real-Time Measuring of Surface Traction Fields" *IEEE Computer Graphics and Applications*, Vol.25, No.1, pp. 68–75, Jan-Feb, 2005

[3] S. Saga, H. Kajimoto and S. Tachi, "High-resolution tactile sensor using the deformation of a reflection image" *Sensor Review*, Vol. 27, Issue. 1, pp. 35–42, 2007

[4] N. J. Ferrier, and R. W. Brockett "Reconstructing the Shape of a Deformable Membrane from Image Data" *The International Journal of Robotics Research*, Vol. 19, No. 9, pp. 795–816, 2000

[5] R. Miyamoto, A. Komatsu, E. Iwase, K. Matsumoto, and I. Shimoyama, "The Estimation of Surface Shape Using Lined Strain Sensors" *Journal of the Robotics Society of Japan*, ROMBUNNO(CDROM), Nov, 2008 (in Japanese)

[6] K. Nagata, M. Ooki, and M. Kakikura, "Feature Detection with an Image Based Compliant Tactile Sensor" *1999 IEEE/RSJ International Conference on Intelligent Robots and Systems*, Vol. 2, pp. 838–843, Oct, 1999

[7] Y. Yamada, Y. Iwanaga, M. Fukunaga, N. Fujimoto, E. Ohta, T. Morizono, and Y. Umetani, "Soft Viscoelastic Robot Skin Capable of Accurately Sensing Contact Location of Objects" *Proc. of IEEE/RSJ/SICE Int. Conference on Multisensor Fusion and Integration for Intelligent Systems*, pp. 105–110, Aug, 1999

[8] G. Obinata, D. Ashis, N. Watanabe and N. Moriyama, "Vision Based Tactile Sensor Using Transparent Elastic Fingertip for Dexterous Handling" *Mobile Robots: Perception & Navigation*, pp. 137–148, 2007

[9] Y. Ito, Y. Kim and G. Obinata, "Slippage Degree Estimation for Dexterous Handling of Vision-Based Tactile Sensor" *In Proceedings of 2009 IEEE Conference on Sensors*, pp. 449–452, Oct, 2009

[10] Y. Ito, Y. Kim , C. Nagai and G. Obinata, "Shape Sensing by Vision-based Tactile Sensor for Dexterous Handling of Robot Hands" *In Proceedings of 2020 IEEE Conference on Automation Science and Engineering*, Aug, 2010 (to be published)